Juha Heiskala, Kalle Kotilahti, Lauri Lipiäinen, Petri Hiltunen, P. Ellen Grant, and Ilkka Nissilä. 2007. Optical tomographic imaging of activation of the infant auditory cortex using perturbation Monte Carlo with anatomical a priori information. In: Brian W. Pogue and Rinaldo Cubeddu (editors). Diffuse Optical Imaging of Tissue. Proceedings of SPIE, volume 6629, paper 66290T, 11 pages.

http://dx.doi.org/10.1117/12.728276

Optical tomographic imaging of activation of the infant auditory cortex using perturbation Monte Carlo with anatomical a priori information

Juha Heiskala*[abc], Kalle Kotilahti[bc], Lauri Lipiäinen[bc], Petri Hiltunen[bc], P. Ellen Grant[de], and Ilkka Nissilä[bc]

[a]BioMag Laboratory, HUSLAB, Helsinki University Central Hospital, P.O. Box 340, FI-00029 HUS, Finland

[b]Laboratory of Biomedical Engineering, Helsinki University of Technology, P.O. Box 2200, FI-02015 HUT, Finland

[c] Helsinki Brain Research Center, University of Helsinki, P.O. Box 13, FI-00014, Finland

[d] Massachusetts General Hospital, Department of Pediatric Radiology, Boston, Massachusetts 02114, USA

[e] Athinoula A. Martinos Center for Biomedical Imaging, Massachusetts General Hospital, 149 13th St., Charlestown, MA 02129, USA

ABSTRACT

We have developed a perturbation Monte Carlo method for calculating forward and inverse solutions to the optical tomography imaging problem in the presence of anatomical *a priori* information. The method uses frequency domain data. In the present work, we consider the problem of imaging hemodynamic changes due to brain activation in the infant brain. We test finite element method and Monte Carlo based implementations using a homogeneous model with the exterior of the domain warped to match digitized points on the skin. With the perturbation Monte Carlo model, we also test a heterogeneous model based on anatomical *a priori* information derived from a previously recorded infant T1 magnetic resonance (MR) image. Our simulations show that the anatomical information improves the accuracy of reconstructions quite significantly even if the anatomical MR images are based on another infant. This suggests that significant benefits can be obtained by the use of generic infant brain atlas information in near-infrared spectroscopy and optical tomography studies.

Keywords: Optical imaging, NIRS, tomography, Monte Carlo

1. INTRODUCTION

Diffuse optical tomography is a non-invasive medical imaging modality that uses near-infrared (NIR) and visible red light. Information of optical properties within the tissue being imaged are drawn from measurements of light that has traveled through the tissue.

In its simplest form, optical imaging can be performed using a single light source and a single detector, measuring the intensity of radiation that passes through tissue. Changes in optical properties in tissue between the source and the detector can be seen as changes in the signal intensity. As measurements with long source-detector distances contain more information from photons that travel deep in the tissue than measurements with short distances, multiple measurements with different source-detector distances can be used for depth resolution.

In optical tomography, the goal is to determine the distribution of optical properties or their changes within the tissue. To solve this inverse problem, multiple overlapping measurements are needed. Measuring

*Juha.Heiskala@iki.fi, phone +358 9 47175542

either the distribution of photon flight times (time domain measurement) or phase shift in an intensity modulated signal (frequency domain measurement) is essential for the determination of background optical properties and can also be helpful in depth discrimination.

In order to solve the inverse problem of optical tomography (the imaging problem), a solver for the forward problem (simulation of the propagation of light in tissue) is needed. This requires a model that can predict the measured signal when the measurement geometry and optical properties of tissue are known. Propagation of near-infrared light in tissue can be modeled by the radiative transfer equation (RTE). Much used methods to solve the forward problem include the numerical solution of the diffusion approximation (DA) of the RTE, usually using the finite element method (FEM) and Monte Carlo (MC) methods. In the present paper we mainly use the MC method as a forward model. While slower to run on a computer than implementations using FEM and the DA, the MC method has the advantage that it solves the RTE accurately, and is easily adapted to allow arbitrary geometries. In particular, the non-scattering clear regions such as the cerebrospinal fluid (CSF) can be correctly modeled. MC also allows easy integration of *a priori* knowledge of optical properties. The heavy calculational burden of MC currently prohibits reconstruction of optical parameters using iterative solutions of the forward problem (nonlinear optimization), but perturbation Monte Carlo (pMC) methods have been demonstrated to be effective in localizing changes or perturbations in optical properties.[1,2]

We present a novel 3D voxel-based pMC method which uses frequency domain data. The voxel-based implementation of the pMC method allows modeling arbitrary geometries. We use an infant head model based on MR imaging to localize brain activations and also plan to use it also to detect anomalies in perfusion. Due to safety concerns, MR imaging can only be obtained on patients likely to benefit from the imaging. Optical imaging can be applied to a much wider range of subjects. We are developing methods to apply MR image data obtained on patients to the wider subject population. In this work, we digitized the cardinal landmarks, the positions of the optical fibers, and many other points on the subject's scalp and used these to warp the anatomical model (obtained from another infant) to match the geometry of the infant under the current study.

We test the effectiveness of the pMC method using *a priori* anatomical knowledge and a simulated absorption perturbation in the brain, and reconstruct the change in μ_{a} using a) a heterogeneous model with anatomical a priori information, and b) a model with homogeneous optical properties. The results of the two cases are then compared.

We use the methods presented to reconstruct HbR and HbO_2 changes from the measurement data of an infant presented with auditory stimuli. In addition to the pMC method, a reconstruction using the measured data is also calculated using the TOAST software based on FEM and the DA.[3]

2. METHODS

2.1 Modeling

2.1.1 Frequency domain perturbation Monte Carlo

In MC, detailed information about the light propagation in tissue is obtained by tracing paths of individual photons or photon packs as they travel within the tissue. The path length l of a photon between scattering events is drawn from an exponential distribution with a probability distribution $\exp(-\mu_s l)$, where μ_s is the scattering coefficient in the tissue. After each scattering event a new propagation direction for the photon pack is drawn from a phase function, in our case the Henyey-Greenstein[4] phase function. Absorption of light is handled at each scattering event or after a short pre-defined distance if photon path before scattering is longer than this distance. Weight of the photon pack is reduced by multiplying with $\exp(-\mu_a l_{abs})$, where μ_a is the absorption coefficient and l_{abs} is the length of the path traveled since the weight was last reduced. The rules of photon propagation are well explained in previous literature,[4,5] and we shall not go into detail here. In our MC implementation,[6] the tissue is divided into volume elements (voxels), each of which may have different optical properties.[7]

In the pMC method, a sensitivity map is created by accumulating data of the regions visited by photons on their way from a source to a detector. This allows us to estimate the change that a perturbation in optical properties in a certain position will have on the measured signal. Since the changes in cerebral blood flow in brain activation imaging mainly cause changes in the absorption, we only consider those in the current work, although changes in scattering may also occur.[8]

In our MC simulation, a photon pack starts with weight 1. After traveling a distance l in a region with absorption coefficient μ_a the weight is reduced as $\exp(-\mu_a l)$.[6]

Signal intensity seen by a detector is given by

$$W = \sum_{phot} w_{phot} = \sum_{phot} \exp[-\sum_{r} \mu_a(r) l_{r,phot}], \tag{1}$$

where w_{phot} is the intensity contribution of a photon pack, and $\mu_a(r)$ and $l_{r,phot}$ are the absorption coefficient and photon path length in region r of the tissue. The sum in the exponential function goes over all regions r.

Differentiating equation 1 with respect to the absorption coefficient in a region ρ yields

$$\frac{\partial W}{\partial \mu_a(\rho)} = \sum_{phot} -l_{\rho,phot} \exp[-\sum_{r} \mu_a(r) l_{r,phot}], \tag{2}$$

which allows the estimation of the sensitivity of the intensity measurement to an absorption change in a region ρ. Here we assume that modulation amplitude and DC intensity measurement types are interchangeable, as our modulation frequency (100 MHz) is relatively small.

The phase shift φ is obtained from MC simulation as

$$\varphi = \operatorname{atan}(\frac{y}{x}) \tag{3}$$

$$y = \sum_{phot} \exp(-\sum_{r} \mu_a(r) l_{r,phot}) \sin(2\pi f T_{phot}) \tag{4}$$

$$x = \sum_{phot} \exp(-\sum_{r} \mu_a(r) l_{r,phot}) \cos(2\pi f T_{phot}) \tag{5}$$

where x and y are the components of complex fluence, and the sum goes over all photons. f is the modulation frequency and T_{phot} is the total flight time of the photon.

Differentiating the above formulae with respect to μ_a in region ρ we obtain

$$\frac{\partial \varphi}{\partial \mu_a(\rho)} = \frac{1}{1+(\frac{y}{x})^2}(\frac{1}{x}\frac{\partial y}{\partial \mu_a(\rho)} - \frac{y}{x^2}\frac{\partial x}{\partial \mu_a(\rho)}) \tag{6}$$

$$\frac{\partial y}{\partial \mu_a(\rho)} = \sum_{phot} -l_{\rho,phot} \exp(-\sum_{r} \mu_a(r) l_{r,phot}) \sin(2\pi f T_{phot}) \tag{7}$$

$$\frac{\partial x}{\partial \mu_a(\rho)} = \sum_{phot} -l_{\rho,phot} \exp(-\sum_{r} \mu_a(r) l_{r,phot}) \cos(2\pi f T_{phot}) \tag{8}$$

Accumulating data of the region specific path lengths traveled by photons contributing to the complex fluence allows us to estimate (7) and (8). Sensitivity maps thus obtained give the rate of change in phase shift in each region ρ in response to change in $\mu_a(\rho)$ in that region.

Combining the above results, we can use MC simulations to accumulate sensitivity maps that give an estimate of the rate of change in both signal intensity and phase shift in response to change in absorption.

The reconstructions of perturbations in μ_a are done by minimizing the squared difference

$$E = \sum_{s,d} [\frac{1}{\sigma_{\log[W_{EXP}]}} (\Delta \log[W_{MC}(s,d)] - \Delta \log[W_{EXP}(s,d)])^2 \quad + \\ \frac{1}{\sigma_{\varphi_{EXP}}} (\Delta\varphi_{MC}(s,d) \quad - \quad \Delta\varphi_{EXP}(s,d))^2] \tag{9}$$

where the sum goes over all sources s and all detectors d. $\Delta \log[W_{EXP}]$, $\Delta \log[W_{MC}]$ and $\sigma_{\log[W_{EXP}]}$ are the change in logarithm of signal intensity observed experimentally and predicted by MC simulation, and the experimental variance of logarithm of signal intensity. $\Delta\varphi_{EXP}$, $\Delta\varphi_{MC}$ and $\sigma_{\varphi_{EXP}}$ are the changes in phase shift observed experimentally and predicted by MC, and the variance of phase data observed experimentally. The reconstruction is performed by calculating the gradient of E as a function of $\mu_a(\rho)$ in the different regions ρ. The $\mu_a(\rho)$ are iteratively updated in the direction of the negative gradient until a minimum has been reached.

2.1.2 Diffusion approximation solution with finite elements

Solving the DA of the RTE using finite elements is a widely used method for solving the forward problem of optical tomography. A major advantage of the method is the computational speed which allows iterative solution of the inverse problem by updating the optical parameters and recalculating the forward solution repeatedly. Non-linear optimization methods can be used for solving the inverse problem.

A disadvantage of the method is its inability to correctly model clear regions such as CSF. Also, the quality of the mesh used can influence the outcome. We used the TOAST software developed at University College London[3] to calculate the FEM based reconstructions.

In this work, FEM reconstruction was done using a mesh with 18929 elements. The reconstruction used linear basis functions and had 4458 degrees of freedom. The TOAST software uses Gauss-Newton algorithm for reconstruction and Tikhonov regularization.[3] The regularization parameter was set at $\alpha = 10^{-6}$.

2.1.3 Anatomical model

Both the pMC method described above and the TOAST software require anatomical models in which the forward problem is calculated and the reconstruction of change in optical properties is done.

Anatomical data were derived from MR imaging of neonates. The T1-weighted images were collected using a 1.5 Tesla Signa Scanner by GE Medical Systems.[9] The MR images were segmented into tissue classes including the scalp, skull, gray and white brain matter and the CSF.

Table 1. Optical properties of tissue types[11,12]

Tissue type	$\mu_s(\text{mm}^{-1})$	g	$\mu_a(\text{mm}^{-1})$	n
Scalp	10	0.9	0.018	1.3
Skull	18	0.9	0.016	1.3
Gray matter	5	0.9	0.048	1.3
White matter	10	0.9	0.037	1.3
Subarachnoid CSF	0.027	0.9	0.0041	1.3
Ventricular CSF	0.01	0.9	0.0041	1.3

Since we do not have anatomical MR images of the particular subjects studied with optical measurements, a segmented MR image of another neonate was deformed to correspond to the head of the studied infant. For this, recorded coordinates of surface points including locations of optical fibers on the infant's scalp were used. Among the recorded points were special landmark points that were also identified in the MR image

Figure 1. Digitizing the landmark points. The infant is wearing a black fiber holder made of thermoplastic material, attached using elastic tissue.

being deformed. Software developed in VTT Information Technology and the Laboratory of Biomedical Engineering at Helsinki University of Technology[10] was used to calculate a free form deformation that matched the anatomical landmark points from measurement and the MR image and deformed surface of the head to correspond to digitized surface points. The deformation thus obtained was then used for deforming the voxel based anatomical model. The resulting anatomical model, while not identical to a model based on MR imaging of the subject that was studied, can be expected to contain some of the same anatomical features.

Starting values for optical parameters of the tissue classes were obtained from literature[11,12] (see Table 1). These values were then iteratively updated from the starting values so that the data calculated using the model corresponded to measurement results.

2.2 Experimental methods

We used optical imaging to study hemodynamic changes in the neonatal auditory cortex in response to auditory stimuli. A group of three healthy neonates (gestational ages 40-45 weeks, weights 3030-3930 grams, head circumference 33-36 cm) were measured.

Sinusoidal tones at the standard (1 kHz) and the deviant frequencies (1.25 kHz) with two upper harmonics were used as stimuli. The duration of each stimulus was 100 ms including 5-ms rise and fall times. A stimulus train consisted of eight beeps (20% deviants), which were presented with loudspeakers with a 700-ms interstimulus interval. The sound intensity was 60 dB. The length of the stimulus train was 5 s, which was followed by a rest period of 5-25 s. The stimulus train was repeated 18 times per one run, and up to 5 runs were recorded during an experiment. The stimuli were controlled with the Presentation software.[13]

A 16-channel frequency-domain instrument was used for this study.[14] An adaptable fiber holder made of a thermoplastic material was used to attach the optodes to the head of the infant (Fig. 1). Two source fibers were used, just above each ear, and eight detector fiber bundles were attached in two arcs around the source fiber, four at a distance of 15 mm and four at a distance of 25 mm from the source. Two wavelengths (685 and 830 nm) were used and the optical power entering the tissue was between 4 and 5mW. The intensity and the phase of the photon density wave were calculated with a software lock-in amplifier and sampled at 11.5 Hz. Drift and slow oscillations were removed from the data by using a high-pass filter (-3 dB cutoff frequency 0.026 Hz). The data were interpolated to a frequency of 10 Hz.

The heart rate and the arterial oxygen saturation were recorded using a pulse oximeter in an anesthesia monitor (S/5 Compact Anesthesia Monitor, Datex-Ohmeda, Helsinki, Finland). The pulse oximetry sensor

(FlexSat, Datex-Ohmeda) was attached to the right foot of the infant. An accelerometer was used to record the movements of an infant during the measurement.

Locations on the scalp of the infant including three landmark points (left and right preauricular points and nasion and locations of the optical fibers) were digitized using the Polhemus Fastrack[15] system (see Fig. 1). Soft plastic was used to cover the sharp point of the digitizing pen in order to avoid hurting the infant.

2.3 Simulation

Simulations offer a controlled way to evaluate the performance of the reconstruction methods described above.

We ran MC simulations using an array of optical sources and detectors that was identical to the one used in the experiment. Activation of the auditory cortex was modeled by a local increase in absorption coefficient μ_a in the auditory cortex. Simulations were carried out with and without this increase to produce difference data between the two cases. We then reconstructed the change in μ_a from the simulated difference data. Our anatomical models consisted of cubical voxels with side length 0.86 mm, and the sensitivity maps used in the reconstructions were calculated dividing the volume into cubical subregions with side length 1.72 mm or double the side length of voxels in the anatomical model. Different situations were considered as explained below.

Two anatomical models based on MR imaging of two neonates were used, one to generate the simulated data, and the second generate the sensivitity maps that were needed to to solve the inverse problem. This procedure was used to simulate the uncertainty in the anatomy that is present in the experimental situation. Anatomical landmark points and points on the surface of the anatomical model were identified. The second anatomical model was deformed to match the first, using the marked points. This deformed model was then used for image reconstruction from the simulated data analogously to the experimental case.

We will refer to the anatomical model in which the simulated measurements were calculated as the digital phantom and to the second model that was used for calculating the sensitivity maps needed by the pMC method as the deformed model.

The reconstructions were calculated using a) the deformed head model and the correct optical parameters, and b) the deformed head model with both μ_a and μ_s 10% higher and c) lower than in the model that was used to generate the simulated data.

The results were compared with results obtained using the digital phantom with the correct optical parameters (i.e. the same model that was used for generating the simulated measurement). This corresponds to the unrealistic situation in which the anatomy and baseline optical properties are known perfectly.

Results were also compared with reconstruction obtained using the deformed head model and homogeneous optical parameters. The homogeneous parameters were adjusted so that the forward solution produced results that matched the data obtained using the digital phantom as well as possible. While a perfect match between a heterogeneous and a homogeneous model was not possible, we were able to match the results to within 10% in logarithmic signal intensity and phase shift.

To test the usefulness of phase information for the pMC reconstruction, reconstruction using the digital phantom with correct optical parameters was calculated without using phase information.

3. RESULTS

3.1 Simulation

Successful image reconstruction in optical tomography requires multiple overlapping measurements. In this work, a simple grid designed for studying brain physiology and hemodynamics was used. We wanted to see how reconstruction results would change using varying degree of *a priori* anatomical knowledge with this topographical setup. We were also interested in knowing how useful frequency domain data would be in tomographic reconstruction.

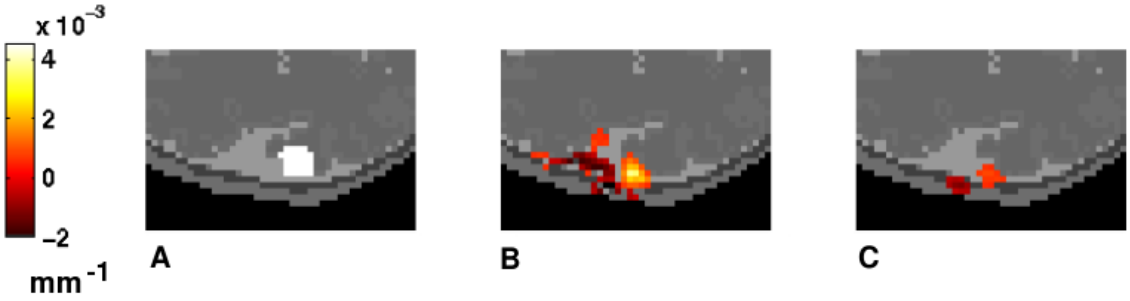

Figure 2. Reconstruction results from a simulated measurement using the perturbation shown in A. Magnitude of the perturbation is $6\times10^{-3}\text{mm}^{-1}$. In B. reconstruction using intensity and phase information and in C. the result obtained using only intensity information. Results are shown superimposed over brain anatomy.

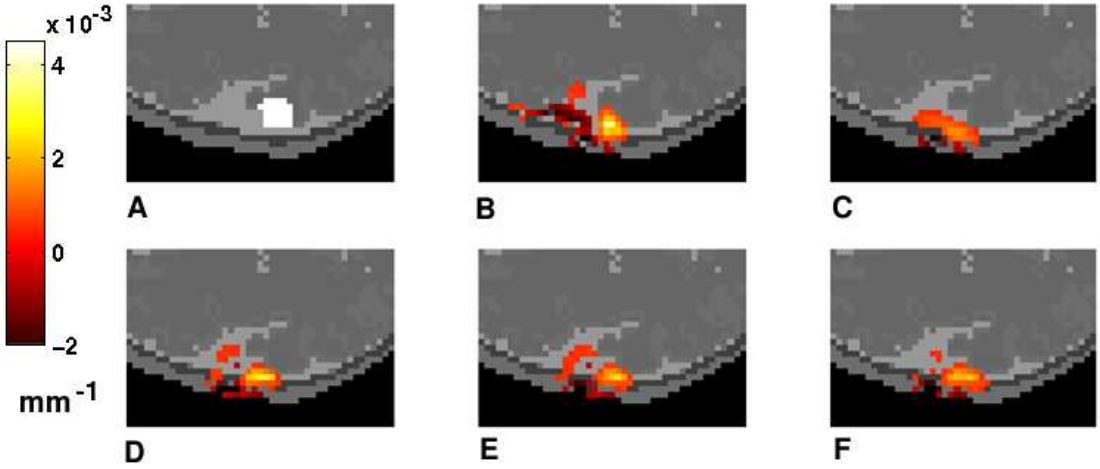

Figure 3. Reconstruction results from a simulated measurement. A transaxial slice at the level of the center of the perturbation is shown, superimposed on brain anatomy. A. Actual change in μ_a is 6×10^{-3} B. Reconstruction using original MRI, C. Reconstruction done using homogeneous background parameters, D. Reconstruction using MR data from another individual, deformed to correspond in surface form to the subject of the simulated measurement, and correct optical parameters, E. reconstruction done using deformed head model and parameters which are 10% lower than actual μ_a and μ_s, F. reconstruction done using deformed head model and parameters which are 10% higher than actual μ_a and μ_s.

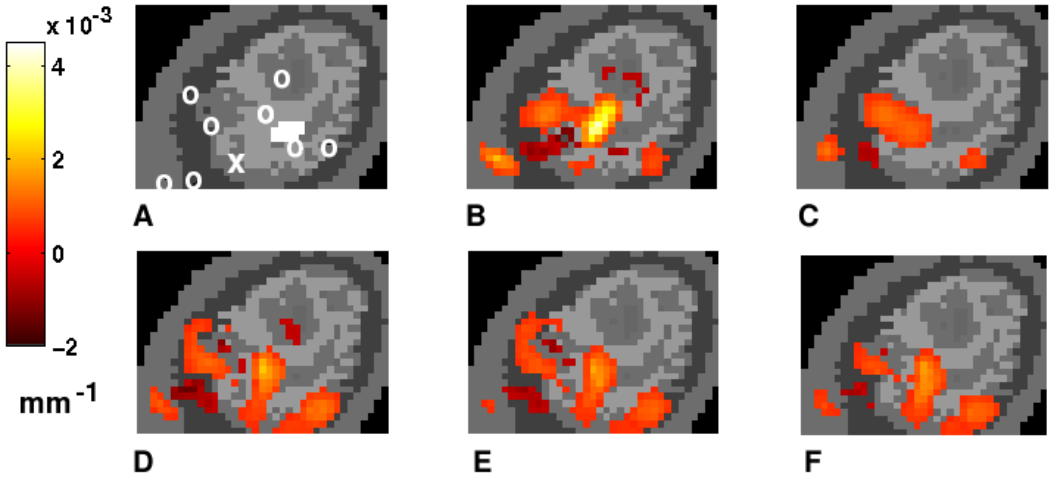

Figure 4. Reconstruction results from a simulated measurement. A sagittal slice at level corresponding to the superficial part of the perturbation is shown. A. Actual change in μ_a is 6×10^{-3}. Projection to plane of the location of the source fiber marked with X, detector fibers marked by circles. B. Reconstruction using original MRI, C. Reconstruction done using homogeneous background parameters, D. Reconstruction using MR data from another individual, deformed to correspond in surface form to the subject of the simulated measurement, and correct optical parameters, E. reconstruction done using deformed head model and parameters which are 10% lower than actual μ_a and μ_s, F. reconstruction done using deformed head model and parameters which are 10% higher than actual μ_a and μ_s.

An absorptive perturbation was placed in the auditory cortex of our digital phantom, and simulated measurements were performed to obtain difference data between situations with and without the perturbation. The perturbation had magnitude $6\times10^{-3}\text{mm}^{-1}$ above the baseline μ_a, and was centered at depth of approximately 13 mm from skin surface. It included all brain tissue within 6 mm from the center.

In Fig. 2 we show the reconstruction results obtained when the digital phantom which was used to produce the simulated difference data was also used as the anatomical model for producing the sensitivity maps needed for the reconstruction. In Fig. 2 B the reconstruction result obtained using both intensity and phase shift data is shown. Fig. 2 C shows the result obtained using only intensity data. Comparing these results to the correct result shown in Fig. 2 A shows that using phase data significantly aids the reconstruction. The contrast of the reconstructed perturbation is higher and closer to the true value when both phase and intensity data are used. On the other hand, there are more falsely reconstructed negative absorption changes. In this example, we studied reconstructing a localized perturbation in the presence of statistical noise of the order of 0.5%. In lower contrast-to-noise situations, noise may reduce the effectiveness of phase information in the reconstruction.

In Figs. 3 and 4 transaxial and sagittal slices of the 3D reconstruction results from the simulated experiment are shown. Reconstruction results obtained using varying degrees of anatomical *a priori* knowledge are shown. As seen in Figs. 3 B and 4 B, the reconstruction is successful in localizing the perturbation when perfect knowledge of anatomy and baseline optical properties are available. The reconstruction places the perturbation slightly more superficially than in the correct solution shown in Fig. 3 A. Also by comparing images A and B of Fig. 4 one can see that in the reconstruction the perturbation is spread out. This is largely due to the fact that the fiber array shown superimposed in Fig. 4 A does not provide sufficient information to accurately localize a perturbation that falls in between measurements, as in here.

In Figs. 3 D-F and 4 D-F, slices of the reconstruction results obtained using the deformed model for calculating sensitivity maps are shown. In image D in both Figures, slices of results obtained using sensitivity maps calculated with the deformed head model and correct optical properties are shown. In both Figures,

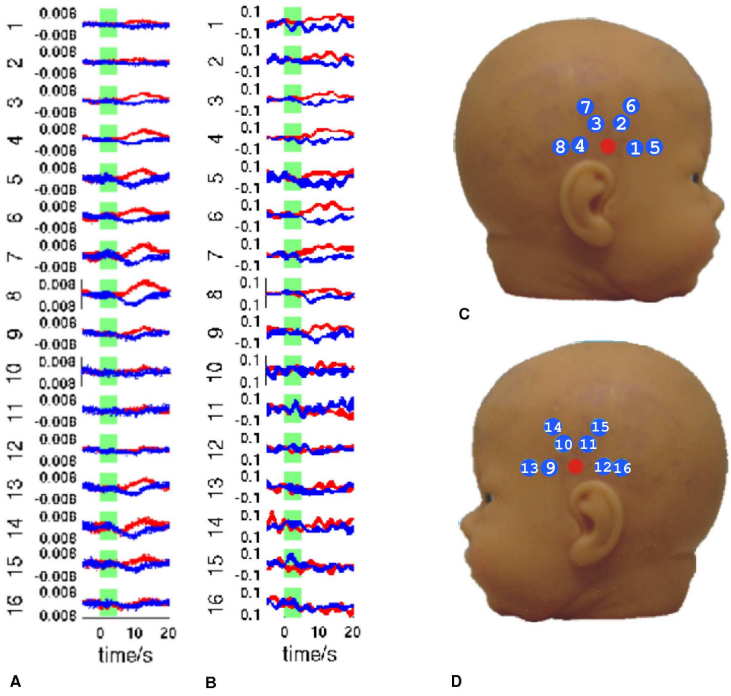

Figure 5. Averaged responses from a single infant. Time course of A. change from baseline in signal intensity (log10 scale) and B. change in phase shift (degrees) in response to an auditory stimulus. Wavelength $\lambda = 685nm$ shown in blue, $\lambda = 830nm$ in red. Thickness of the graphs represent standard error. The timing of the stimulus train is shown in green. Channel numbers shown on the left hand side of each graph correspond to the detector numbers which are shown in images C. and D. The sources are located above each ear, marked with red dots.

image E shows reconstruction result obtained using sensitivity maps that were calculated using the deformed anatomical model and μ_a and μ_s that were 10% lower than those used for producing the simulated data. In image F in both Figures, results are shown that were obtained using the deformed anatomical model and μ_a and μ_s that were 10% higher than those for producing the simulated data. Figures 3 C and 4 C show reconstruction results obtained using the deformed model and homogeneous optical parameters for creating the sensitivity maps.

The results show that the perturbation is reconstructed more accurately with the deformed heterogeneous model than with a homogeneous model, and the results remain fairly good also when 10% error is introduced in μ_a and μ_s. It is worth mentioning that the homogeneous parameters were adjusted so that the simulation using these parameters produces very similar results as our simulated measurement using the heterogeneous head model, and in fact a simulation using our homogeneous parameters matches more closely results of our simulated measurement than a simulation using the heterogeneous parameters that are increased or reduced by 10%. Naturally, in our example the ratio of optical properties between different tissues was preserved also when 'wrong' optical parameters were used. In reality, the ratio is of course not exactly known and must be determined from the data.

3.2 Experiment

In Fig. 5 the averaged time courses of change in signal intensity and phase shift in response to an auditory stimulus are presented for one infant. Results for the other two infants were similar. Responses are shown for the two wavelengths 685 nm and 830 nm.

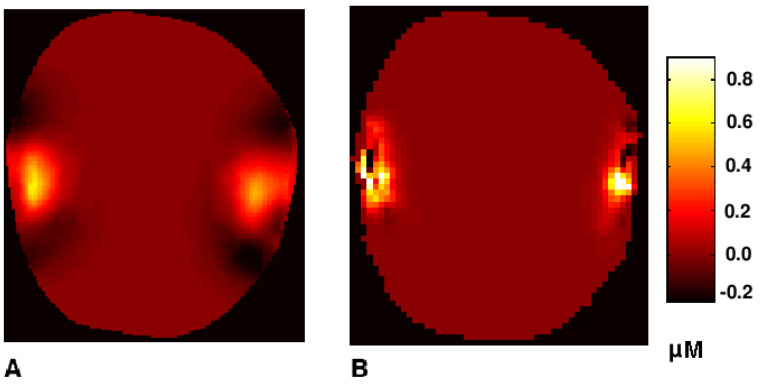

Figure 6. Change in oxygenated hemoglobin concentration reconstructed using A. FEM and B. pMC method (in micromolars). A transaxial slice at the height of the light sources is shown.

The data show that responses are generally larger in measurements with the longer source-detector separation, suggesting a deep source.

Absorption changes were reconstructed from the experimental data using FEM and the pMC method for the two wavelengths. Difference from baseline of intensity and phase data at 10 seconds after stimulus onset were used as input. For pMC reconstruction, a heterogeneous model obtained by deforming a segmented MR image to correspond to the subject was used. For the FEM reconstruction, the same anatomical model with homogeneous background optical properties was used. The background optical properties were iteratively adjusted so that a simulation using them and the deformed anatomical model matched the experimental data as closely as possible. The absorption changes in the two wavelengths were converted to changes in the concentrations of oxygenated an deoxygenated hemoglobin using specific absorption coefficients for oxygenated and deoxygenated hemoglobin for the wavelengths used.[16]

The results obtained for the change in concentration of oxygenated hemoglobin using pMC and FEM are presented in Fig. 6. It can be seen that the pMC method produces a more localized reconstruction with the bulk of the absorption change in the superficial regions of the brain. In the FEM solution the reconstructed absorption change is spread to a wider area, with a lower peak change in absorption.

4. DISCUSSION

In this paper we presented a pMC method that makes use of both signal intensity and phase shift data for the reconstruction of absorption changes in tissue. The method allows the use of an arbitrary anatomical model. We demonstrated that using anatomical data derived from another individual than the one being studied can improve the quality of reconstructed absorption images significantly. We used a deformation that matched the surface of the anatomical model with the surface points of our subject. Our results suggest that even a rudimentary approach to using a priori information can work. More refined deformation algorithms that preserve essential anatomical properties of the brain and the development of methods of averaging anatomical information from several subjects is likely to improve the results further, and yield methods that any group working on optical imaging of infants is likely to benefit from. We also showed that our experimental auditory paradigm yields measurable changes in signal intensity and phase shift over the infant auditory cortex, and that phase information is important in the reconstruction even if the perturbation is present only in the absorption coefficient.

ACKNOWLEDGEMENTS

The authors wish to thank Juha Koikkalainen of VTT Information Technology for his help with deforming MR images and Leena Wallendahr of Cognitive Brain Research Unit, University of Helsinki for her help in conducting the experiments. Financing from the KAUTE Foundation, Instrumentarium foundation, the Finnish Cultural Foundation, the Finnish Academy of Science and Letters and the Jenny and Antti Wihuri Foundation are acknowledged.

REFERENCES

1. C. Hayakawa, J. Spanier, F. Bevilacqua, A. Dunn, J. You, B. Tromberg, V. Venugopalan, "Perturbation Monte Carlo methods to solve inverse photon migration problems in heterogeneous tissues," *Optics Letters* **26** (2001)
2. Y. Phaneendra Kumar, R. M. Vasu, "Reconstruction of optical properties of low-scattering tissue using derivative estimated through perturbation Monte-Carlo method", *Journal of Biomedical Optics* **9** (2004)
3. M. Schweiger, S. R. Arridge, and I. Nissilä, " Gauss-Newton method for image reconstruction in diffuse optical tomography," *Physics in Medicine and Biology* **50**, 2365-2386 (2005).
4. L. Wang, S. L. Jacques and L. Zheng, "MCML-Monte Carlo modeling of light transport in multi-layered tissues," *Computer Methods and Programs in Biomedicine*, **47**, 131-146 (1995)
5. S. A. Prahl, M. Keijzer, S. L. Jacques, and A. J. Welch, "A Monte Carlo model of light propagation in tissue," in *Dosimetry of Laser Radiation in Medicine and Biology,* G. J. Müller and D. H. Sliney, eds., *SPIE Institute Series* **5**, 102-111 (1989)
6. J. Heiskala, I. Nissilä, T. Neuvonen, S. Järvenpää, and E. Somersalo, "Modeling anisotropic light propagation in a realistic model of the human head," *Applied Optics,* **44**, 2049-2057 (2005)
7. D. A. Boas, J. P. Culver, J. J. Stott and A. K. Dunn, "Three dimensional Monte Carlo code for photon migration through complex heterogenous media including the adult human head," *Optics Express*, **10,** 159-170 (2002)
8. J. Heiskala, K. Kotilahti, I. Nissilä, "An application of perturbation Monte Carlo in optical tomography," *Proceedings of the 27th Annual International Conference of the IEEE Engineering in Medicine and Biology Society* (2005)
9. General Electric Company, 3135 Easton Turnpike, Fairfield, CT 06828-0001, USA
10. J. Koikkalainen and J. Lötjönen, "Reconstruction of 3-D head geometry from digitized point sets: an evaluation study,"*IEEE Transantions on Information Technology in Biomedicine*, **8,** 377-386 (2004)
11. F. Schmidt, *Development of a time-resolved optical tomography system for neonatal brain imaging*, PhD thesis, University of London (1999)
12. Y. Fukui, Y. Ajichi, and E. Okada, "Monte Carlo prediction of near-infrared light propagation in realistic adult and neonatal head models," *Appl. Opt.* **42,** 2281-2287 (2003)
13. Neurobehavioral Systems online, www.neurobs.com
14. I. Nissilä, T. Noponen, K. Kotilahti, and T. Katila, L. Lipiäinen, T. Tarvainen, M. Schweiger and S. Arridge, "Instrumentation and calibration methods for the multichannel measurement of phase and amplitude in optical tomography," *Review of Scientific Instruments* **76**, 044302 (2005)
15. Polhemus Inc, 40 Hercules Drive, P.O. Box 560 Colchester, VT 05446, USA
16. M. Cope, *The Application of Near Infrared Spectroscopy to Non Invasive Monitoring of Cerebral Oxygenation in the Newborn Infant*, PhD Thesis, University College London (1991)